A Hybrid Mesh Free Local RBF- Cartesian FD Scheme for Incompressible Flow around Solid Bodies

A. Javed, K. Djidjeli, J. T. Xing, S. J. Cox

***Abstract*—**A method for simulating flow around the solid bodies has been presented using hybrid meshfree and mesh-based schemes. The presented scheme optimizes the computational efficiency by combining the advantages of both meshfree and mesh-based methods. In this approach, a cloud of meshfree nodes has been used in the domain around the solid body. These meshfree nodes have the ability to efficiently adapt to complex geometrical shapes. In the rest of the domain, conventional Cartesian grid has been used beyond the meshfree cloud. Complex geometrical shapes can therefore be dealt efficiently by using meshfree nodal cloud and computational efficiency is maintained through the use of conventional mesh-based scheme on Cartesian grid in the larger part of the domain. Spatial discretization of meshfree nodes has been achieved through local radial basis functions in finite difference mode (RBF-FD). Conventional finite difference scheme has been used in the Cartesian 'meshed' domain. Accuracy tests of the hybrid scheme have been conducted to establish the order of accuracy. Numerical tests have been performed by simulating two dimensional steady and unsteady incompressible flows around cylindrical object. Steady flow cases have been run at Reynolds numbers of 10, 20 and 40 and unsteady flow problems have been studied at Reynolds numbers of 100 and 200. Flow Parameters including lift, drag, vortex shedding, and vorticity contours are calculated. Numerical results have been found to be in good agreement with computational and experimental results available in the literature.

***Keywords*—**CFD, Meshfree particle methods, Hybrid grid, Incompressible Navier Strokes equations, RBF-FD.

I. Introduction

MESHFREE or meshless methods have emerged as a new class of numerical techniques during past few years. One of the common characteristics of these methods is that they eliminate, at least, the structure of the mesh by approximating the solution over a set of arbitrarily distributed data points (or nodes) [4]-[9]. There is no requirement pre-selected connectivity or relationship amongst the nodes of meshless domain. Meshfree methods can also deal with complex geometries and irregular boundaries more efficiently. Moreover, computational ease of adding or removing nodes from the domain is another attractive advantage of meshless methods. Meshless methods therefore have the potential to alleviate the mesh generation complexities arising in traditional methods like Finite Difference (FD), Finite Volume (FV) and Finite Element (FE) methods and significantly reduce the computational cost associated with grid generation. Due to these features, meshless methods have become one of the hottest areas of research in computational fluid dynamics [12]-[19]. However, despite their stated advantages, meshless methods possess overall lesser computational efficiency than traditional mesh based methods like FD, FV and FD [21]. This in fact, is the major limitation which impedes the wide applicability of meshless methods [11].

Radial Basis Functions (RBFs) have been used for many years for multivariate data and function interpolation. In 90s, use of RBFs was proposed for the solution of Partial Differential Equations (PDEs) [25]. Lately there has been great interest of researchers to use RBFs for solution of PDEs on irregular domains by collocation approach [12], [25]-[27]. Local RBF methods have also been proposed to overcome the ill-conditioning problem associated with dense, large sized matrices. Local RBFs compromise on spectral accuracy and produce well-conditioned and sparse linear systems which are capable of efficiently handling the non-linearities[17]. These methods are therefore considered well suited for fluid dynamics problems which involve large number of data points in meshfree domains. RBF in Finite Difference Mode (RBF-FD) is a local RBF method which was independently proposed by Tolstykh et al. [29] and Wright et al. [30] for different set of applications. RBF-FD allows the use of Finite Difference method on randomly distributed data points (or nodes). The method has been successfully applied to various fluid dynamics problems involving incompressible Navier Strokes equations [27], [32].

Like other Meshfree methods, RBF based methods also suffer from high computational cost compared with conventional mesh based methods. For example, calculation of RBF weights corresponding to the neighbouring particles of a data point requires expensive square root and matrix inversion processes. Moreover, calculation of derivative approximation at a given order of accuracy usually requires much more number of neighboring particles (or nodes) for meshfree methods on irregular grid than for finite difference methods on Cartesian grid. As a result, the bandwidth of matrices representing the governing algebraic equations greatly expands in case of meshfree methods [11]. Therefore, the iteration process is slowed down due to relatively dense matrix equations and the computational efficiency is reduced. At the same time, meshfree methods have the advantage to efficiently deal with complex geometry.

Conventional mesh-based methods (e.g. FD, FV and FE methods) offer better computational efficiency over

A. Javed is with CED Group, Faculty of Engineering and Environment, University of Southampton, SO171BJ, Southampton, United Kingdom(Phone +44-7534354285, e-mail: A.Javed@soton.ac.uk).

K. Djidjeli, J. T. Xing, and S. J. Cox are with CED Group, Faculty of Engineering and Environment, University of Southampton, SO171BJ, Southampton, United Kingdom (e-mail: kkd@soton.ac.uk, jtxing@ soton.ac.uk, sjc@soton.ac.uk).

meshfreemethods. However, generation of an efficient mesh, which could ensure accurate results, is generally a tedious and time consuming task. Cartesian grid is generally considered to be much more efficient to generate but it cannot be applied to complex geometries. In order to cope with this problem, coupled multi-grid methods have been proposed [33]-[35]. However these methods rely on interpolation approximations at the grid interchanges and suffer from inaccuracies especially when high gradients exist at these junctures. Some researchers have also proposed the use of Cartesian grids on irregular shapes using boundary-fitted methods [36]-[38]. However, these methods necessitate special treatments close to the boundary and suffer from time step restrictions due to small cut cell to accurately embed irregular boundaries in the Cartesian grid. Another approach is to use non-body conformal methods [39], [40] in which a background structured mesh is defined behind the solid boundary. The interface between fluid and solid is traced using 'marker nodes'. These schemes however suffer from inaccuracies coming from accurate tracing of the boundary which is limited by the grid resolution.

In view of the foregone, it is logical to come up with a technique which combines the inherent strengths of both meshfree and mesh-based methods. Here, a hybrid technique is presented to simulate incompressible flow around arbitrarily shaped solid objects. The proposed technique couples RBF-FD method on meshfree zone around the solid body and conventional Finite difference method applied to the Cartesian grid zone in rest of the domain. Meshfree nodes efficiently adapt to the irregular shape of the solid boundary. Outer boundary of the meshfree zone is a regular rectangular or squared shaped. A Cartesian mesh can therefore be generated and coupled to the outer boundary of meshfree zone as shown in Fig. 1. Computationally expensive RBF-FD method is therefore limited to only small meshfree zone of the computational domain where it is required to deal with irregularly shaped solid boundaries. The remaining computational domain is dealt with conventional finite difference method on a Cartesian grid which enjoys computational efficiency over its meshfree counterpart. Values of field variables at collocation points on meshfree boundary serve as boundary conditions for Cartesian grid zone. Therefore, an overall efficient solution scheme is achieved which can effectively handle irregularly shaped solid boundaries.

TABLE I
COMMON RADIAL BASIS FUNCTIONS $\phi(r)$

Re	St
Multiquadric (MQ)	$\phi(r) = \sqrt{r^2 + \sigma^2}$
Inverse Multiquadric (IMQ)	$\phi(r) = 1/\sqrt{r^2 + \sigma^2}$
Inverse Quadric (IQ)	$\phi(r) = 1/(r^2 + \sigma^2)$
Gaussian (GA)	$\phi(r) = \exp(-(\sigma r)^2)$

II. FORMULATION OF PROBLEM

A. Governing Equations

Incompressible, transient, viscous Navier-Strokes equations in non-dimensional pressure-velocity form are expressed as:

$$\nabla.\vec{V} = 0 \quad (1)$$

$$\partial\vec{V}/\partial t = -\nabla P - (\vec{V}.\nabla)\vec{V} + (1/Re)\nabla^2\vec{V} \quad (2)$$

where $\vec{V}$ is the velocity vector, P is the pressure, and Re is the Reynolds number. The equations are discretized using time implicit RBF-FD method proposed by Javed et al [41]. The method has been shown to be stable and produce accurate results in the regions of gradients high field variables. Detail of temporal and spatial discretization is described below.

B. Time Splitting

Time splitting of the governing equations has been achieved using implicit fractional step method [41]. In this method, convective term of momentum equation is treated with 2nd order explicit Adam-Bashforth scheme whereas viscous term is decomposed using 2nd order implicit Crank-Nicholson scheme [42].

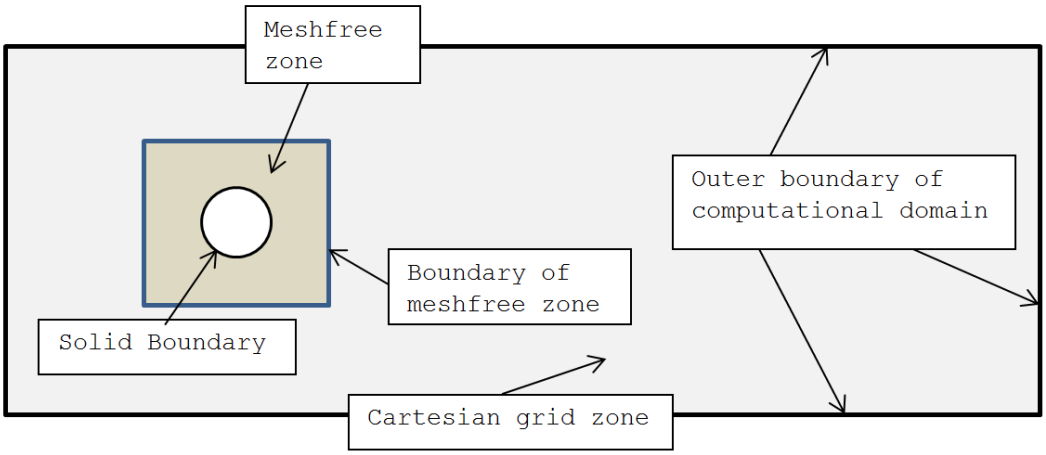

Fig. 1 Schematic of Hybrid Meshfree-Meshed Domain

Equation (2) therefore assumes the following form:

$$(\vec{V}^* - \vec{V}^n)/\partial t = -1/2\left[3(\vec{V}^n.\nabla)\vec{V}^n - (\vec{V}^{n-1}.\nabla)\vec{V}^{n-1}\right] + 1/(2Re)\left[\nabla^2(\vec{V}^n + \vec{V}^*)\right] \quad (3)$$

Superscripts n and $n-1$ represent the iteration number and V^*represents the intermediate velocity. The pressure term appearing in momentum (2) can be linked with velocity as:

$$(\vec{V}^{n+1} - \vec{V}^*)/\partial t = -\nabla P^{n+1} \quad (4)$$

Now, from continuity condition (1):

$$\nabla.\vec{V}^{n+1} = 0 \quad (5)$$

Substituting the value of $\vec{V}^{n+1}$from (4) into (5) leads to,

$$\nabla^2 P^{n+1} = (1/\Delta t)\nabla.\vec{V}^* \quad (6)$$

Equation (6) is called pressure Poisson equation. By incorporating pressure term into continuity equation, the continuity is satisfied in the process of solution of transient flow problem.

C. Space Splitting

As mentioned before, space splitting has been achieved using RBF-FD in meshfreezone.RBF in finite difference mode (RBF-FD) is the generalization of classical finite difference method over scattered data points (or nodes) using Radial Basis Functions. The standard RBF interpolation for a set of distinct points$x_j \epsilon \mathbb{R}^d, j = 1,2, \ldots N$ is given by [32]:

$$u(x) \approx s(x) = \sum_{j=1}^{N} \lambda_j \phi\left(\left||x - x_j|\right|\right) + \beta \quad (7)$$

where, $\phi\left(\left||x - x_j|\right|\right)$is a radial basis function, $||.||$is a standard Euclidean norm and $\beta and \lambda_j$ are expansion coefficients. Some of the common radial basis functions are given in Table I. r is the radial distance between two data points and σ is the shape function. Equation (7) can be written in Lagrange form as:

$$\bar{s}(x) = \sum_{j=1}^{N} \mathcal{X}\left(\left||x - x_j|\right|\right) u(x_j) \quad (8)$$

where, $\mathcal{X}\left(\left||x - x_j|\right|\right)$is of the form (7) and satisfies the cardinal conditions as

$$\mathcal{X}\left(\left||x_k - x_j|\right|\right) = \begin{cases} 1, if k = j \\ 0, if k \neq j \end{cases} k = 1,2, \ldots . n \quad (9)$$

Applying a differential operator $\mathcal{L}$ on (8) at node x_1, as shown in Fig. 2, yields:

$$\mathcal{L}u(x_1) \approx \mathcal{L}\bar{s}(x_1) = \sum_{j=1}^{n} \mathcal{L}_{\mathcal{X}}\left(\left||x_1 - x_j|\right|\right) u(x_j) \quad (10)$$

Using classical finite difference approach, the derivative of any parameter u at any node, sayx_1, can be expressed as weighted linear sum of same variable values at surrounding nodes in the support domain. Therefore,

$$\mathcal{L}u(x_1) = \sum_{j=1}^{N} w_{(1,j)}^{(\mathcal{L})}\, u(x_j) \quad (11)$$

where$N$ is the number of nodes in the support domain of nodex_1, $u(x_j)$is the value of parameter $u$at node $x_j$and $w_{(1,j)}^{(\mathcal{L})}$ is the weight of corresponding differential operator $\mathcal{L}$ at node $x_j$for node $x_1$as shown in Fig. 2. Comparing (10) and (11), the weights$w_{(1,j)}^{(\mathcal{L})}$can be written as:

$$w_{(1,j)}^{(\mathcal{L})} = \mathcal{L}_{\mathcal{X}}\left(\left||x_1 - x_j|\right|\right) \quad (12)$$

In practice, RBF weights can be computed by solving the following linear system [27]:

$$\begin{bmatrix} \Phi & e \\ e^T & 0 \end{bmatrix}\begin{bmatrix} \boldsymbol{w} \\ \mu \end{bmatrix} = \begin{bmatrix} \mathcal{L}\Phi_1 \\ 0 \end{bmatrix} \quad (13)$$

where $\mathcal{L}\Phi_1$represents the column vector $\mathcal{L}\phi = [\mathcal{L}\phi(||x - x_1||\ \mathcal{L}\phi(||x - x_2|| \ldots . \mathcal{L}\phi(||x - x_n||]^T$evaluated at node x_1 and μ is a scalar parameter which enforces the condition:

$$\sum_{j=1}^{n} w_{(1,j)}^{(\mathcal{L})} = 0 \quad (14)$$

Evaluation of (13) at each node, sayx_1, gives weights $w_{(1,j)}^{(\mathcal{L})}$of all the nodes in the support domain for particular differential operator $\mathcal{L}$. Corresponding weights and locations of nodes in support domains are then used to approximate the complete differential equation at nodex_1. The procedure repeated to approximate the differential equations at all the node in domain.

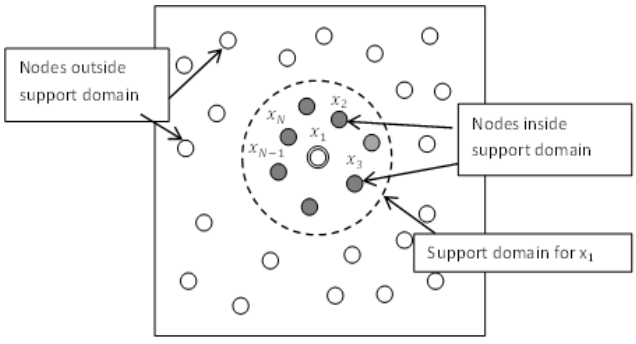

Fig. 2 Support domain of a reference node

Classical finite difference method has been used in Cartesian grid zone to improve computational efficiency of the solution. At time iteration n, 1st and 2nd spatial derivatives of a variable u, with respect to x, can be approximated at node (i,j) using central difference schemes on a standard 2-D Cartesian grid (see Fig. 3) as follows:

$$\left.\frac{\partial u^n}{\partial x}\right|_{(i,j)} \approx \frac{u^n_{i+1,j} - u^n_{i-1,j}}{2\Delta x} \tag{15}$$

$$\left.\frac{\partial^2 u^n}{\partial x^2}\right|_{(i,j)} \approx \frac{u^n_{i+1,j} - 2u^n_{i,j} + u^n_{i-1,j}}{\Delta x^2} \tag{16}$$

Spatial discretization is to be decided by corresponding meshfree / Cartesian zone of the particular node. Separate Matrix equations can be formulated, for meshfree and Cartesian nodes, by writing governing equations ((3) and (6)) in discretized form at each node of the domain. Solution of these equations results nodal pressure and intermediate velocity values at each time step. Subsequently, velocity values at next time iteration can be calculated using (4).

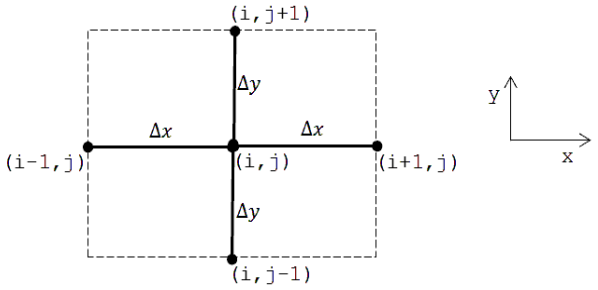

Fig. 3 Nodes on standard 2-D Cartesian grid

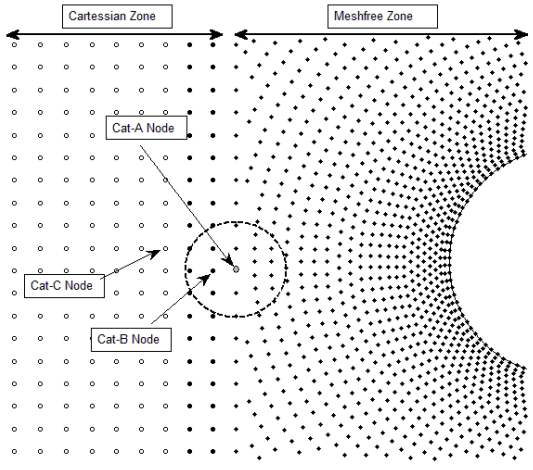

Fig. 4 Coupling of Meshfree-Cartesian Zones

D. Treatment of Computational Domain

As mentioned earlier, the computational domain has been divided into two zones namely Cartesian and meshfree zones. Meshfree zone comprises of a nodal cloud. The inner boundary of this nodal cloud adapts to the shape of solid boundary whereas the outer boundary of nodal cloud is essentially rectangular for 2-D domain. Beyond the nodal cloud, a standard Cartesian grid exists. A closed view of computational domain near the juncture of the two zones is shown in Fig. 4. The nodes existing in the domain can be classified in three categories. Cat-A nodes fall in the meshfree zone and are treated with RBF-FD method. Value of field variable at each node is calculated using the linear weighted sum of corresponding values at the nodes in the support domain. Near the outer boundary of the meshfree zone, the support domain of Cat-A nodes may extend to the Cartesian zone. Therefore, some Cartesian nodes will also fall in the support domain of these meshfree nodes. These Cartesian nodes which fall in the support domain of meshfree nodes, are named as Cat-B nodes in Fig. 4. Although Cat-B nodes influence the results of corresponding meshfree nodes, solution at Cat-B nodes is calculated using conventional finite difference method. On the contrary, Cat-C nodes are those Cartesian nodes which do not fall in the support domain of any meshfree (Cat-A) node. Outer Boundary nodes of meshfree zone are positioned in a way that they can be treated as boundary nodes for Cartesian grid. Thus the values calculated at these nodes serve as boundary conditions for Cartesian grid at corresponding time iteration.

At every time step, the solution is first calculated at meshfree zone. For this calculation, the boundary conditions at the solid surface and field variable values at Cat-B nodes are used. After having calculated the results in meshfree zone, standard finite difference scheme is used to calculate results in Cartesian zone. For this, nodes at the outer boundary of meshfree cloud provide the boundary conditions to Cartesian nodes. In addition to this, the boundary conditions at outer boundaries of domain are also used.

III. Numerical Tests

A. Calculation of Order of Accuracy

Spatial Accuracy of the presented method has been found by simulating the decaying vortex on hybrid grid. Analytical solution of decaying vortex case is known. Therefore, the test is often used by researchers to verify the accuracy of new methods [21], [42], [44], [45]. Theoretical expressions for velocity and pressure fields for this case are given by:

$$u(x,y,t) = -\cos(\pi x)\sin(\pi y)\exp(-2\pi^2 t/Re) \tag{17}$$

$$v(x,y,t) = \sin(\pi x)\cos(\pi y)\exp(-2\pi^2 t/Re) \tag{18}$$

$$p(x,y,t) = -0.25[\cos(2\pi x) + \sin(2\pi y)]\exp(-4\pi^2 t/Re) \tag{19}$$

Here, Re is the flow Reynolds number which is taken as $Re = \rho u_0 L/\mu$ (ρ is the flow density, u_0 is the maximum velocity at t=0, μ is the dynamic viscosity and L is the length of the vortex). Numerical simulations are carried out on a rectangular domain with dimensions [-0.5x0.5]x[-0.5x0.5].

The central region of the rectangle with dimensions [-0.25x0.25]x[-0.25x0.25] comprises of meshfree zone. The surrounding domain is represented by Cartesian nodes as shown in Fig. 5. Randomness has been introduced in meshfree zone by disturbing the meshfree nodes from their original (Cartesian) positions. However, in order to maintain uniformity in distribution of meshfree nodes, perturbation in the position of meshfree nodes has been limited to 20% of the grid spacing. Three layers of Cat-B nodes have been introduced outside the meshfree zone.

The initial conditions are introduced at each node of the domain using the velocity and pressure values obtained from (32)-(34) at t=0. Dirichlet boundary conditions are imposed on all the four boundary using theoretical expressions at given time values. The values of field variables for subsequent time iterations are calculated at inner nodes using the method outlined in Section II. The time step value is chosen to be 10^{-5} sec. Flow Reynolds number is set as Re=10. Simulation is run for duration of 0.4 sec. The error is calculated by comparing the numerical results with theoretical values obtained by evaluating (32)-(34) at each node. Spatial accuracy is calculated by changing the grid size and calculating norm-2 of the error for pressure and velocity values. The plot of error values for changing grid size is shown in Fig. 6. The slope of error versus grid size curve on a logarithmic plot yields the order of spatial accuracy of the method. The order of accuracy is 3.95 for pressure and 3.8 for velocity.

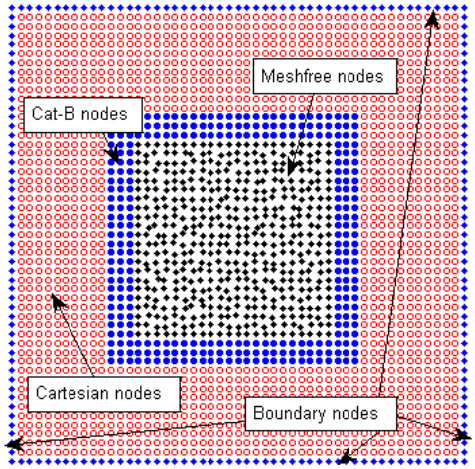

Fig. 5 Grid used for Accuracy Test

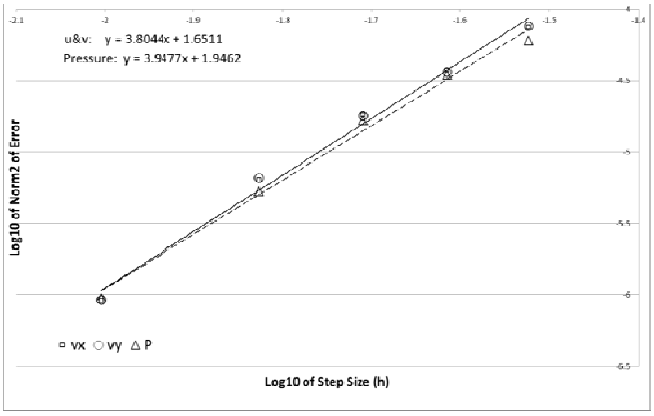

Fig. 6 Order of Accuracy in Space

B. Flow around Cylinder

Validation of presented numerical method has been demonstrated by simulating steady and unsteady flows around cylindrical body. The problem has been studied by various researchers [2], [11], [20]-[22], [31], [43]. Therefore, sufficient reliable data is available in the literature, for various cases, to compare with. The flow around cylindrical objects remains steady at low Reynolds numbers$(Re < 49)$. However an oscillating Vortex Street (known as Kamran Vortex) is observed behind the cylinder, at higher values of Reynolds number$(49 \leq Re \leq 200)$, making the problem unsteady. Reynolds number is calculated as $Re = \rho UD/\mu$, whereρ is the fluid density, U is the free stream velocity, D is the diameter of the cylinder and μ is the dynamic viscosity of the fluid. Configuration of problem is shown in Fig. 7. The circular body represents the cross section of cylindrical object in a 2-D domain. The upper and lower walls are at a distance of $16D$. The Inlet and outlet boundaries are kept at distances of $8D$ and $30D$ from the center of the cylinder respectively. This ensures that the flow at the solid boundary is not affected by the boundary conditions at outer domain boundaries. Lengths of sides of the meshfree domain are 3 times the diameter of cylinder. Therefore, meshfree zone constitutes only 1.35% of the total domain size.

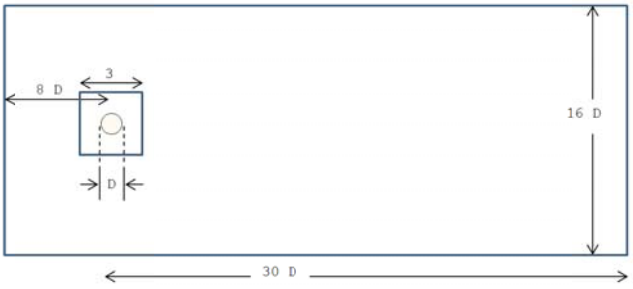

Fig. 7 Configuration of 2-D Domain for simulation of flow around cylindrical objects

TABLE II
COMPARISON OF SEPARATION ANGLE (θ_{sep}), LENGTH OF RECIRCULATION REGION (L_{sep}) AND DRAG COEFFICIENT (CD) AT RE 10, 20 AND 40

Re	Source	θ_{sep}	L_{sep}	C_D
10	Dennis and Chang [1]	29.6	0.265	2.85
10	Takami and Keller [3]	29.3	0.249	2.80
10	Taunn and Olson [20]	29.7	0.25	3.18
10	Ding et al [18]	30.0	0.252	3.07
10	He and Doolen[23]	26.9	0.237	3.17
10	Mei and Shyy[24]	30.0	0.249	-
10	Guo et al [28]	31.6	0.267	-
10	Chew et al [21]	28.6	0.28	3.09
10	Firoozjaee et al [31]	-	0.26	-
10	Present Study	30.47	0.255	3.12
20	Dennis and Chang [1]	43.7	0.94	2.05
20	Takami and Keller [3]	43.7	0.935	2.01
20	Taunn and Olson [20]	44.1	0.9	2.25
20	Ding et al [18]	44.1	0.93	2.18
20	He and Doolen[23]	42.9	0.921	2.152
20	Mei and Shyy[24]	42.1	0.902	-
20	Guo et al [28]	42.3	0.935	-
20	Chew et al [21]	44.2	0.95	2.19
20	Firoozjaee et al [31]	-	0.94	-
20	Fornberg[43]	-	0.91	2.00
20	Present Study	44.11	0.91	2.20
40	Dennis and Chang [1]	53.8	2.35	1.52
40	Takami and Keller [3]	53.6	2.32	1.54
40	Taunn and Olson [20]	54.8	2.1	1.68
40	Ding et al [18]	53.5	2.20	1.71
40	He and Doolen[23]	53.8	2.245	1.50
40	Mei and Shyy[24]	50.12	2.19	-
40	Guo et al [28]	53.13	2.2	-
40	Chew et al [21]	53.47	2.3	1.59
40	Firoozjaee et al [31]	-	2.26	-
40	Fornberg[43]	-	2.24	1.50
40	Present Study	53.13	2.18	1.63

Inflow boundary conditions ($u = U, v = 0$, where U is the free stream velocity) are applied at the inlet. No slip boundary conditions ($u = v = 0$) have been introduced at the solid boundary. No slip boundary condition implies that $\partial p/\partial n = 0$ (where n is the outward normal direction to the boundary). Therefore, Neumann boundary conditions for pressure are introduced at solid boundary. At the outlet, outflow boundary conditions are met using the expression $\partial u/\partial t + \partial u/\partial x = 0$. At top and bottom boundary, $\partial u/\partial y = 0, v = 0$ is applied.

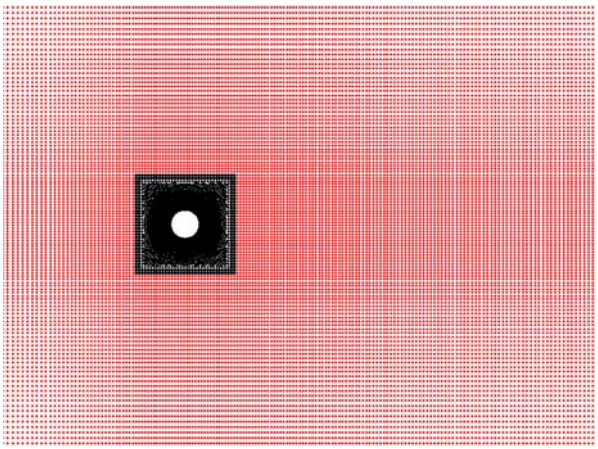

(a) Nodes in Cartesian and meshfree zones

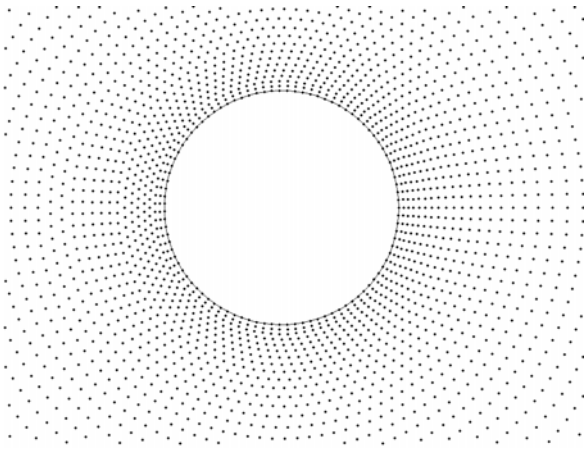

(b) Orthogonal nodal arrangement around solid boundary

Fig. 8 Grid around circular cylinder

The nodal arrangement used for the problem is shown in Fig. 8 (a). A total of 100 nodes are placed on the circular solid boundary. The domain is represented by 2895 meshfree nodes (arranged radially) and 32088 Cartesian nodes. Therefore, computationally expensive meshfree scheme will be used at only 8.3% nodes of the domain. In order to implement Neumann boundary condition at solid boundary, first two layers of nodes around the solid are arranged orthogonally with the boundary nodes as shown in Fig. 8 (b). The condition of orthogonal grid at the outlet boundary is naturally satisfied due to Cartesian grid.

Lift and drag forces at the solid boundary are evaluated by summing up vertical and horizontal components of pressure and viscous forces at all the boundary nodes as shown in Fig. 9. Lift (F_L) and drag (F_D)forces can therefore be expressed as:

$$F_L = \rho U^2 \left(\sum_{i=1}^{n_s} \left(-P_i \sin\theta_i \, r d\theta + \frac{1}{Re} \omega_i \cos\theta_i \, d\theta \right) \right) \quad (20)$$

$$F_D = \rho U^2 \left(\sum_{i=1}^{n_s} \left(-P_i \cos\theta_i \, r d\theta - \frac{1}{Re} \omega_i \sin\theta_i \, d\theta \right) \right) \quad (21)$$

where P_i and ω_i are the pressure and vorticity values at boundary node i, n_s is the number of nodes at solid boundary, r is the radius of circle, θ_i is the angular position of the node i from horizontal (as shown in Fig.9) and $d\theta$ is the angular displacement between two consecutive boundary nodes. The lift and drag coefficients (C_D and C_L) around the solid boundary are then evaluated using following expressions:

$$Lift\ coefficient = C_L = \frac{F_L}{\rho U^2} \quad (22)$$

$$Drag\ coefficient = C_D = \frac{F_D}{\rho U^2} \quad (23)$$

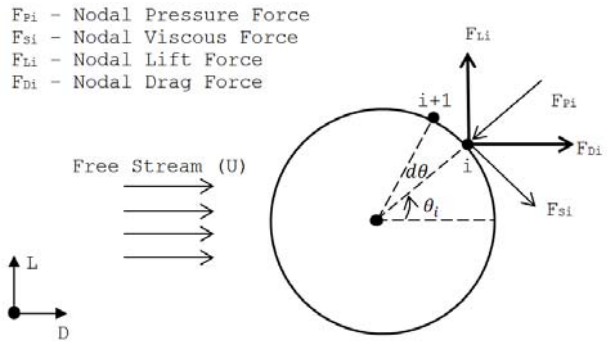

Fig. 9 Lift and drag force vectors on solid boundary

The steady flow cases have been studied at Re 10, 20 and 40. Time step is kept as $5x10^{-3}$ sec. The simulation is run until steady state is achieved. Vorticity profiles of flow at all the three Reynolds numbers are shown in Fig. 10. The resultant values of drag coefficients, separation angles and lengths of recirculation regions have been calculated and validated against the solutions from previous researchers [1], [3], [20], [23], [24], [28], [31], [43]. Comparison of results has been presented in Table II. The resultant flow parameters are found to be in good agreement with the results of previous researchers at the three Reynolds numbers.

TABLE III
COMPARISON OF LIFT AND DRAG COEFFICIENTS (C_L AND C_D) AND STOUHAL NUMBER (ST) AT RE 100 AND 200

Re	Source	C_L	C_D	St
100	Braza et al [2]	±0.25	1.364±0.015	0.160
100	Lieu et al [10]	±0.34	1.350±0.012	0.164
100	Ding et al [11]	±0.28	1.325±0.008	0.164
100	C.Shu et al [21]	±0.34	1.362±0.010	0.166
100	Present Study	±0.36	1.35±0.01	0.166
200	Belovetal[22]	±0.64	1.19±0.042	0.193
200	Braza et al [2]	±0.75	1.40±0.05	0.200
200	Lieu et al [10]	±0.69	1.31±0.049	0.192
200	Ding et al [11]	±0.60	1.327±0.045	0.196
200	C.Shu et al [21]	±0.34	1.325±0.008	0.192
200	Present Study	±0.72	1.354±0.058	0.196

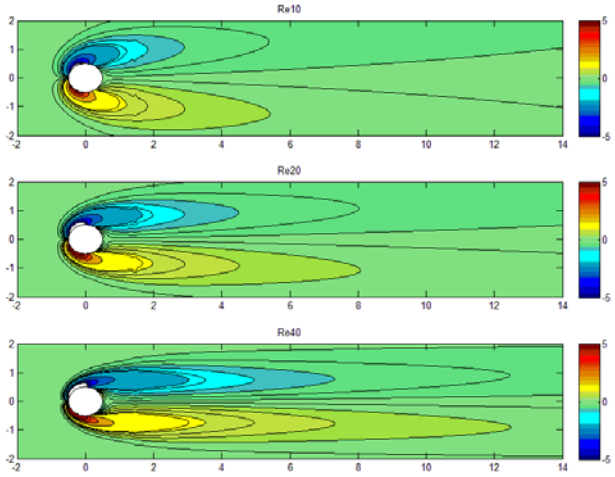

Fig. 10 Vorticity profiles at Re 10, 20 and 40

In order to simulate unsteady flow around the cylindrical objects, the flow solutions have been calculated at Re100 and 200. Time step has been chosen to be $2.5x10^{-3}$ sec. At these flow conditions, oscillating vortices are obtained behind the solid object. The oscillating vortex profile is captured at various time instances for a complete cycle, and shown in Figs. 11 and 12 for Re 100 and 200, respectively. The oscillatory flow also results in corresponding fluctuation in lift and drag forces over the body. Variation of C_L and C_D has been plotted against time in Figs. 13 and 14 for Re 100 and 200, respectively. It can be observed that magnitude of lift and drag coefficients and frequency of oscillation tend to increase with the increase in Reynolds number. At both Reynolds number, frequency of oscillation of drag coefficient is twice the corresponding oscillation frequency of lift coefficient. Frequency of oscillation can be represented in terms of Strouhal number which is equal to the vortex shedding frequency in case of non-dimensionalized length and time parameters. Therefore, Strouhal number can directly be acquired by frequency of oscillation of C_L versus time plot.

The numerical solutions have been verified by comparing the resultant values of lift and drag coefficients and Strouhal number with results of previous researchers, as shown in Table III. The results show good agreement with the previous solutions [2], [10], [11], [21], [22].

A comparison of computational time between hybrid and fully meshfree schemes was carried out on a grid containing 18026 nodes at flow Reynolds number 100. The simulation was run on Intel ® 3.1 GHz Processor machine and CPU time for every 100 iterations was monitored. Average CPU time for fully meshfree scheme was found to be 468.3 sec compared with the average CPU time of 38.72 sec for Hybrid scheme. Thus the computation time was reduced by almost a factor of 12 with the use of Hybrid scheme. More overdue to fewer meshfree nodes used in Hybrid approach, RBF-FD weight calculation time was also reduced by a factor of 6 compared with fully meshfree approach. Therefore significant improvement in computational time was achieved using hybrid approach.

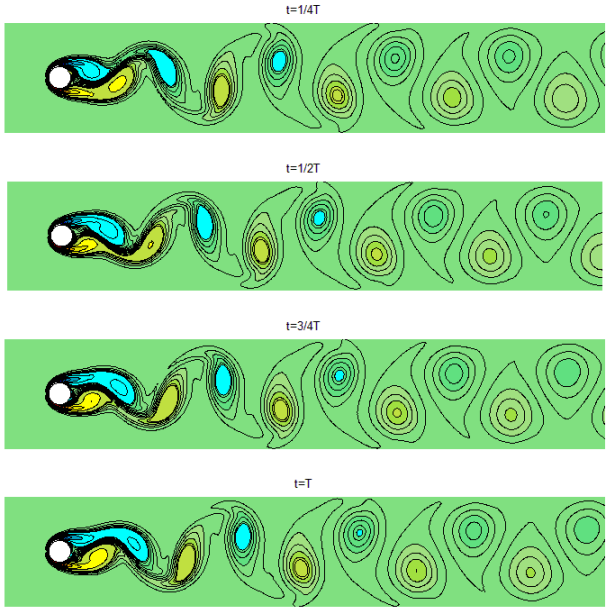

Fig. 11 Vortex shedding at Re 100

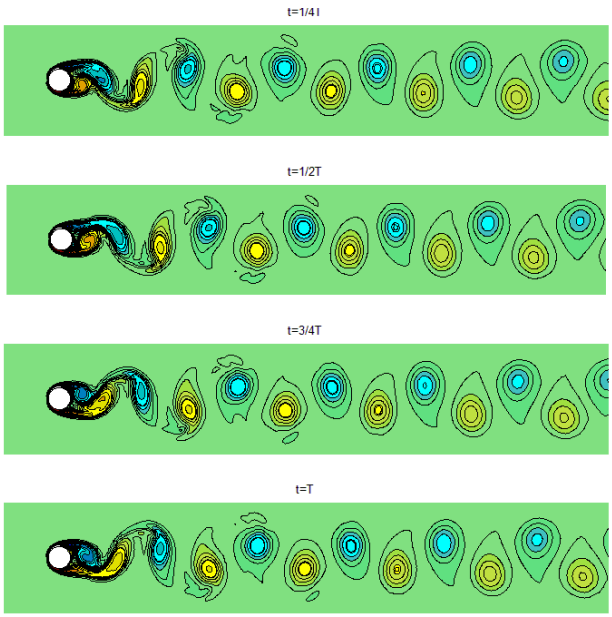

Fig. 12 Vortex shedding at Re 200

IV. Conclusion

RBF-FD is a highly flexible meshless method which is known for accurate and efficient approximation the derivatives of field variables on a meshless domain. However, like other meshless methods, it lacks computational efficiency compared with the conventional mesh based methods. The proposed hybrid scheme therefore couples both the meshless and mesh-based methods on a hybrid grid.

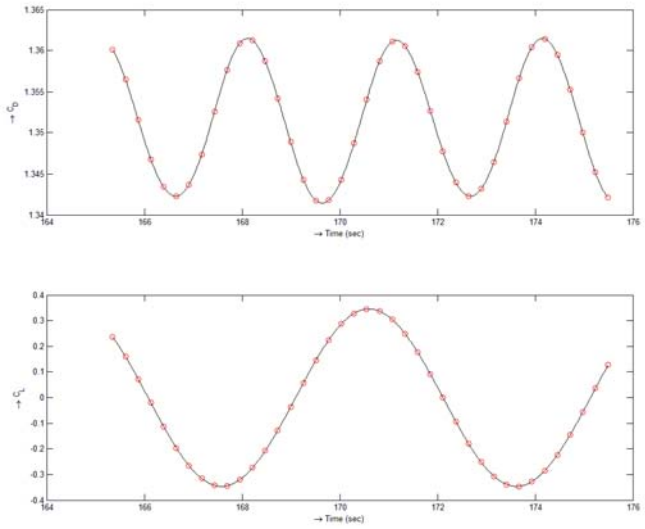

Fig. 13 Variation of C_L and C_D with time at Re 100

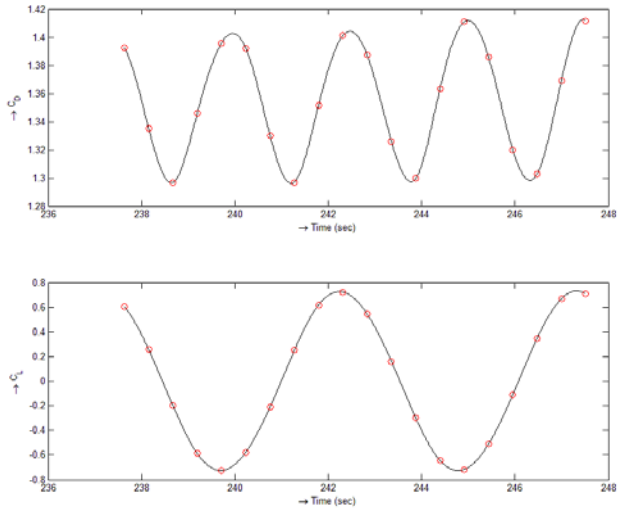

Fig. 14 Variation of C_L and C_D with time at Re 200

The hybrid scheme is used to simulate incompressible flow past circular cylinder. Implicit treatment of time marching is implemented to achieve better stability of the iteration process. The overall hybrid scheme is found to have spatial order of accuracy greater than 3.8 for both pressure and velocity results on a hybrid meshfree-Cartesian grid with rectangular domain. Numerical tests are performed to demonstrate the application of presented method for steady and unsteady flow problems. Accurate solutions have been obtained by using the presented scheme with the use of significantly less computational resources.

References

[1] S. Dennis, and G.-Z. Chang, "Numerical solutions for steady flow past a circular cylinder at Reynolds numbers up to 100," *J. Fluid Mech*, vol. 42, no. 3, pp. 471-489, 1970.

[2] M. Braza, P. Chassaing, and H. H. Minh, "Numerical Study and Physical Analysis of the Pressure and Velocity-Fields in the near Wake

of a Circular-Cylinder," *Journal of Fluid Mechanics*, vol. 165, pp. 79-130, Apr, 1986.

[3] H. Takami, and H. B. Keller, "Steady Two-Dimensional Viscous Flow of an Incompressible Fluid past a Circular Cylinder," *Physics of Fluids*, vol. 12, no. 12, pp. II-51-II-56, 1969.

[4] L. B. Lucy, "A numerical approach to the testing of fission hypothesis," *Astronomical Journal*, vol. 8, pp. 1013-1024, 1977.

[5] B. Nayroles, G. Touzot, and P. Villon, "Generalizing the finite element method: Diffuse approximation and diffuse elements," *Computational Mechanics*, vol. 10, no. 5, pp. 307-318, 1992.

[6] T. Belytschko, Y. Y. Lu, and L. Gu, "ELEMENT-FREE GALERKIN METHODS," *International Journal for Numerical Methods in Engineering*, vol. 37, no. 2, pp. 229-256, 1994.

[7] W. K. Liu, S. Jun, S. F. Li, J. Adee, and T. Belytschko, "Reproducing Kernel Particle Methods for Structural Dynamics," *International Journal for Numerical Methods in Engineering*, vol. 38, no. 10, pp. 1655-1679, May 30, 1995.

[8] J. M. Melenk, and I. Babuska, "The partition of unity finite element method: Basic theory and applications," *Computer Methods in Applied Mechanics and Engineering*, vol. 139, no. 1-4, pp. 289-314, Dec 15, 1996.

[9] E. Onate, S. Idelsohn, O. C. Zienkiewicz, R. L. Taylor, and C. Sacco, "A stabilized finite point method for analysis of fluid mechanics problems," *Computer Methods in Applied Mechanics and Engineering*, vol. 139, no. 1-4, pp. 315-346, Dec 15, 1996.

[10] C. Liu, X. Zheng, and C. Sung, "Preconditioned multigrid methods for unsteady incompressible flows," *Journal of Computational Physics*, vol. 139, no. 1, pp. 35-57, 1998.

[11] H. Ding, C. Shu, K. S. Yeo, and D. Xu, "Simulation of incompressible viscous flows past a circular cylinder by hybrid FD scheme and meshless least square-based finite difference method," *Computer Methods in Applied Mechanics and Engineering*, vol. 193, no. 9-11, pp. 727-744, 2004.

[12] Y. Sanyasiraju, and G. Chandhini, "Local radial basis function based gridfree scheme for unsteady incompressible viscous flows," *Journal of Computational Physics*, vol. 227, no. 20, pp. 8922-8948, Oct, 2008.

[13] J. P. Morris, P. J. Fox, and Y. Zhu, "Modeling low Reynolds number incompressible flows using SPH," *Journal of Computational Physics*, vol. 136, no. 1, pp. 214-226, Sep 1, 1997.

[14] J. J. Monaghan, "Simulating Free-Surface Flows with Sph," *Journal of Computational Physics*, vol. 110, no. 2, pp. 399-406, Feb, 1994.

[15] M. B. Liu, G. R. Liu, and K. Y. Lam, "Constructing smoothing functions in smoothed particle hydrodynamics with applications," *Journal of Computational and Applied Mathematics*, vol. 155, no. 2, pp. 263-284, Jun 15, 2003.

[16] M. Liu, G. Liu, Z. Zong, and K. Lam, "Numerical simulation of incompressible flows by SPH."

[17] C. Shu, H. Ding., and K. S. Yeo., "Computation of Incompressible Navier-Stokes Equations by Local RBF-based Differential Quadrature Method," *Computer Modeling in Engineering and Sciences*, vol. 7, no. 2, pp. 195-206, 2005.

[18] C. Shu, H. Ding, and K. S. Yeo, "Local radial basis function-based differential quadrature method and its application to solve two-dimensional incompressible Navier-Stokes equations," *Computer Methods in Applied Mechanics and Engineering*, vol. 192, no. 7-8, pp. 941-954, 2003.

[19] C. G. Koh, M. Gao, and C. Luo, "A new particle method for simulation of incompressible free surface flow problems," *International Journal for Numerical Methods in Engineering*, vol. 89, no. 12, pp. 1582-1604, Mar 23, 2012.

[20] S.-y. Tuann, and M. D. Olson, "Numerical studies of the flow around a circular cylinder by a finite element method," *Computers & Fluids*, vol. 6, no. 4, pp. 219-240, 12//, 1978.

[21] C. S. Chew, K. S. Yeo, and C. Shu, "A generalized finite-difference (GFD) ALE scheme for incompressible flows around moving solid bodies on hybrid meshfree–Cartesian grids," *Journal of Computational Physics*, vol. 218, no. 2, pp. 510-548, 11/1/, 2006.

[22] A. Belov, L. Martinelli, and A. Jameson, "A new implicit algorithm with multigrid for unsteady incompressible flow calculations," *AIAA paper*, vol. 95, pp. 0049, 1995.

[23] X. He, and G. Doolen, "Lattice Boltzmann method on curvilinear coordinates system: flow around a circular cylinder," *Journal of Computational Physics*, vol. 134, no. 2, pp. 306-315, 1997.

[24] R. Mei, and W. Shyy, "On the finite difference-based lattice Boltzmann method in curvilinear coordinates," *Journal of Computational Physics*, vol. 143, no. 2, pp. 426-448, 1998.

[25] E. J. Kansa, "Multiquadrics - a Scattered Data Approximation Scheme with Applications to Computational Fluid-Dynamics .2. Solutions to Parabolic, Hyperbolic and Elliptic Partial-Differential Equations," *Computers & Mathematics with Applications*, vol. 19, no. 8-9, pp. 147-161, 1990.

[26] J. G. Wang, and G. R. Liu, "On the optimal shape parameters of radial basis functions used for 2-D meshless methods," *Computer Methods in Applied Mechanics and Engineering*, vol. 191, no. 23-24, pp. 2611-2630, 2002.

[27] P. P. Chinchapatnam, K. Djidjeli, and P. B. Nair, "Radial basis function meshless method for the steady incompressible Navier–Stokes equations," *International Journal of Computer Mathematics*, vol. 84, no. 10, pp. 1509-1521, 2007.

[28] Z. Guo, B. Shi, and N. Wang, "Lattice BGK model for incompressible Navier–Stokes equation," *Journal of Computational Physics*, vol. 165, no. 1, pp. 288-306, 2000.

[29] A. I. Tolstykh, and D. A. Shirobokov, "On using radial basis functions in a "finite difference mode" with applications to elasticity problems," *Computational Mechanics*, vol. 33, no. 1, pp. 68-79, Dec, 2003.

[30] G. B. Wright, and B. Fornberg, "Scattered node compact finite difference-type formulas generated from radial basis functions," *Journal of Computational Physics*, vol. 212, no. 1, pp. 99-123, Feb 10, 2006.

[31] A. R. Firoozjaee, and M. H. Afshar, "Steady-state solution of incompressible Navier–Stokes equations using discrete least-squares meshless method," *International Journal for Numerical Methods in Fluids*, vol. 67, no. 3, pp. 369-382, 2011.

[32] P. P. Chinchapatnam, K. Djidjeli, P. B. Nair, and M. Tan, "A compact RBF-FD based meshless method for the incompressible Navier-Stokes equations," *Proceedings of the Institution of Mechanical Engineers Part M-Journal of Engineering for the Maritime Environment*, vol. 223, no. M3, pp. 275-290, Aug, 2009.

[33] C. Perng, and R. Street, "A coupled multigrid-domain-splitting technique for simulating incompressible flows in geometrically complex domains," *International journal for numerical methods in fluids*, vol. 13, no. 3, pp. 269-286, 1991.

[34] M. Hinatsu, and J. Ferziger, "Numerical computation of unsteady incompressible flow in complex geometry using a composite multigrid technique," *International Journal for Numerical Methods in Fluids*, vol. 13, no. 8, pp. 971-997, 1991.

[35] P. Chow, and C. Addison, "Putting domain decomposition at the heart of a mesh-based simulation process," *International journal for numerical methods in fluids*, vol. 40, no. 12, pp. 1471-1484, 2002.

[36] D. Calhoun, "A Cartesian grid method for solving the two-dimensional streamfunction-vorticity equations in irregular regions," *Journal of Computational Physics*, vol. 176, no. 2, pp. 231-275, 2002.

[37] R. B. Pember, J. B. Bell, P. Colella, W. Y. Curtchfield, and M. L. Welcome, "An adaptive Cartesian grid method for unsteady compressible flow in irregular regions," *Journal of computational Physics*, vol. 120, no. 2, pp. 278-304, 1995.

[38] J. Falcovitz, G. Alfandary, and G. Hanoch, "A two-dimensional conservation laws scheme for compressible flows with moving boundaries," *Journal of Computational Physics*, vol. 138, no. 1, pp. 83-102, 1997.

[39] A. Gilmanov, F. Sotiropoulos, and E. Balaras, "A general reconstruction algorithm for simulating flows with complex 3D immersed boundaries on Cartesian grids," *Journal of Computational Physics*, vol. 191, no. 2, pp. 660-669, 2003.

[40] R. Glowinski, T.-W. Pan, and J. Periaux, "A fictitious domain method for external incompressible viscous flow modeled by Navier-Stokes equations," *Computer Methods in Applied Mechanics and Engineering*, vol. 112, no. 1, pp. 133-148, 1994.

[41] A. Javed, K. Djidjeli, and J. Xing, Tang, "Shape adaptive RBF-FD Implicit Scheme for Incompressible Viscous Navier-Strokes Equations," *Journal of Computer and Fluid*, vol. submitted for Publication, 2013.

[42] J. Kim, and P. Moin, "Application of a Fractional-Step Method to Incompressible Navier-Stokes Equations," *Journal of Computational Physics*, vol. 59, no. 2, pp. 308-323, June, 1985, 1985.

[43] B. Fornberg, "A Numerical Study of Steady Viscous-Flow Past a Circular-Cylinder," *Journal of Fluid Mechanics*, vol. 98, no. Jun, pp. 819-855, 1980.

[44] D. Kim, and H. Choi, "A second-order time-accurate finite volume method for unsteady incompressible flow on hybrid unstructured grids," *Journal of Computational Physics*, vol. 162, no. 2, pp. 411-428, 2000.
[45] Y. Zang, R. L. Street, and J. R. Koseff, "A non-staggered grid, fractional step method for time-dependent incompressible Navier-Stokes equations in curvilinear coordinates," *Journal of Computational Physics*, vol. 114, no. 1, pp. 18-33, 1994.

Ali Javedis a PhD research student at Computational Engineering and Design Group, Faculty of Engineering and Environment, University of Southampton, UK. He is a graduate in Aerospace Engineering and has done his Masters in Solid Mechanics before starting the PhD. Presently he is doing research in Meshless Particle Methods and their applications to Fluid Structure Interaction problems. In that, he is investigating the use of local Radial Basis Functions (RBF) for modelling and simulation of flows around fluctuating / moving bodies.

He is also employing Arbitrary LagrangianEulerian (ALE) solution schemes on hybrid meshfree-mesh based grids to develop an efficient solver for analysing flow induced vibrations of cylindrical bodies and aerofoils at various Reynolds Numbers.

Kamal Djidjeli is lecturer in Computational Methods in the Computational Engineering and Design Group, Faculty of Engineering and the Environment at the University of Southampton. He obtained his MSc and PhD degrees in Computational methods from University of West London, Brunel UK in 1988 and 1991. He joined the Faculty of Engineering, University of Southampton in 1991 as Research Fellow and become academic staff Lecturer and Admission Director of Maritime Engineering Science MSc Programme and Exams Officer in the Faculty of Engineering, University of Southampton. DrDjidjeli has over 20 years research experience in the area of numerical analysis and computational engineering. He has published over 50 papers in refereed journals and conferences, and has supervised a number of MSc and PhD students. His current research is on particle meshless methods for fluid flow and fluid structure interaction problems, and energy harvesting. He is a referee for a number of journals, and has undertaken a range of research projects in academia and industry. Dr. Djidjeli serves on the editorial board member of the ISRN Applied Mathematics Journal. He is member of the American Institute of Aeronautics and Astronautics (AIAA), and the Institute of Mathematics and its applications, C. Math, UK.

Jing Tang Zing is an Emeritus Professor in the Fluid Structure Interaction Group, the Faculty of Engineering and the Environment at the University of Southampton. He obtained his doctoral degree in fluid-solid interaction dynamics from Tsinghua University, Beijing China in 1984. He joined the Faculty of Engineering, Mathematics and Science, University of Southampton in 1993. Professor Xing has a broad range of research interests and contributions in theoretical and applied continuum dynamics, computational modelling, fluid-solid interactions and vibration and controls. A major thrust of Professor Xing's current research is in fluid-structure interaction dynamics. He has made significant contributions to the development of the mixed finite element substructure–subdomain method for linear fluid-structure problems, and the mixed finite element – finite difference method for nonlinear fluid-solid interaction modelling. His publication record includes over 200 journal/conference papers and technical research reports. As the principal / a joint investigator of EPSRC and European Projects, he has successfully managed many research grants. He is a fellow of the Institute of Mathematics and its applications, C. Math.

Simon J. Cox is Professor of Computational Methods, Head of the Computational Engineering and Design Research Group and Associate Dean for Enterprise in the Faculty of Engineering and the Environment. He has published over 200 papers. He has a doctorate in Electronics and Computer Science, first class degrees in Maths and Physics and has won over £15Mn in research & enterprise funding, and industrial sponsorship (funding from EPSRC, DTI, TSB, NERC, BBRSC, Microsoft, Intel, Venture Capitalists, and Angel Investors). He has supervised 22 PhD students and manages over 40 Staff in the Computational Engineering and Design Group and Spin-out companies applying and developing high productivity computing in a variety of collaborative interdisciplinary computational science and engineering projects. He is director of the Microsoft Institute for HPC at the University of Southampton, which is working with Microsoft on its future tools, technologies and platforms in the high performance computing, cloud and mobile areas. He has co-founded two Venture Capital based companies: Mesophotonics Ltd (which was sold in 2008) and dezineforce, where he was Chief Scientist (which was sold in 2011).